Fundamental thermal noise in antiresonant hollow-core fibers

Vincent Michaud-Belleau[1], Eric R. Numkam Fokoua[2], Peter Horak[2], Natalie V. Wheeler[2], Shuichiro Rikimi[2], Thomas D. Bradley[3], David J. Richardson[2], Francesco Poletti[2], Jérôme Genest[1], and Radan Slavík[2,*]

[1]*Centre d'optique, photonique et laser, Université Laval, Québec, QC, Canada G1V 0A6*
[2]*Optoelectronics Research Centre, University of Southampton, Southampton, SO17 1BJ, United Kingdom*
[3]*High-Capacity Optical Transmission Laboratory, Eindhoven University of Technology, 5600 MB, Eindhoven, Netherlands*

Fluctuations of the optical length induced by fundamental thermal noise are known to set the ultimate phase resolution of fiber-based interferometers. Although this noise has been studied in detail for optical fibers made of solid glass material, its impact on the performance of hollow-core optical fibers has not yet been assessed. In such fibers, the guided light interacts only weakly with the glass material whose thermal and thermo-optic properties normally determine the thermal noise level, suggesting that a difference in performance should be expected. Based on the comparison of several interferometers optimized for phase sensitivity, we present measurements of thermal noise in the 20 to 200 kHz range in hollow-core nested antiresonant nodeless fibers (NANF) with their core filled with air at different pressures. In this frequency range, our measurements are in good agreement with the adapted thermoconductive noise model we introduce, suggesting that the thermo-optic contribution from the gas that fills the core is generally dominant, regardless of the exact hollow-core fiber design. While we show that an antiresonant hollow-core fiber filled with air at atmospheric pressure is noisier at 1550 nm than a silica fiber of equal optical length and mode-field area, we also demonstrate the lowest thermal noise power per unit optical length ever measured in a fiber ($\approx 1.3 \times 10^{-17}$ (rad^2/Hz)/m at 30 kHz) using a large-mode-area NANF evacuated and sealed at 0.15 atm. In addition to lowering the internal pressure, we predict that the noise density in this spectral range can be reduced by filling the core with a low-polarizability noble gas. Our results indicate that low-loss antiresonant hollow-core fibers can compete with ultrastable cavities for the purpose of laser frequency stabilization; when evacuated, such fibers should constitute the best option to significantly decrease the fundamental noise floor in interferometric applications currently based on conventional solid-core fibers.

I. INTRODUCTION

Optical fibers are widely used in interferometric applications thanks to their flexibility and ultralow loss, which enable the propagation of light over several kilometers in a practical format. Yet, stabilizing the optical path length of a long fiber well within a single wavelength, a typical requirement in interferometry, poses a considerable challenge in the presence of environmental perturbations such as vibrations and temperature drifts. This challenge is especially acute in standard single-mode fiber (SMF) which displays a temperature sensitivity on the order of 10 ppm/K at 1550 nm, dominated by the thermo-optic coefficient of silica (TOC), a relatively large value which often warrants temperature stabilization at the sub-mK level [1,2]. Even when such environmental perturbations are controlled or suppressed, early studies have shown that the optical path length stability of an SMF (related to the phase accumulated by a propagating laser field), just like the propagation time stability (related to the group index), is limited by the thermodynamic motion of the elementary charges in the medium through which light propagates [3,4].

Such fundamental thermal noise, associated to apparent local temperature fluctuations of the fiber, depends on the thermal properties of the fiber material sampled by the optical mode and displays a variance or power which scales with the square of the fiber temperature and with the inverse of the mode volume [5]. Although this scaling with mode volume strongly favors long fibers over, say, whispering gallery mode microresonators [6] or active [7] and passive [8] fiber Bragg gratings (in which a similar fundamental noise is observed), thermal noise in SMF has nonetheless been shown to constitute an important limitation for fiber-optic gyroscopes [9,10], optical fiber links [11,12], optoelectronic oscillators [13], and fiber references used for laser stabilization [14,15]. This is due once again to the relatively large temperature sensitivity of standard SMF, which also describes the conversion of thermodynamic temperature fluctuations to path-length fluctuations or output phase noise [16].

Fundamental thermal noise in SMF can be lowered by increasing the fiber length, which directly increases the mode volume. However, noise reduction appears challenging once the length is maximized in a given application. Increasing the mode-field area also increases the mode volume, but only a modest improvement can be considered before bending loss becomes problematic [17]. Although it complicates

---

*Corresponding author: r.slavik@soton.ac.uk

instrument operation, lowering the fiber temperature appears as the best approach since it reduces both the strength of fundamental thermal noise and the thermal sensitivity in bare SMF [18,19]. However, experimental evidence suggests that temperature reduction may not work well below 150 K as the thermal properties of silica undergo significant changes [20]. Finally, although significant effort has been deployed to reduce the intrinsic low-frequency thermal sensitivity of SMF (relevant for environmental temperature drift), for example, through specialized coatings and jackets [21–23], low-sensitivity fiber supports [24,25], and dopants with negative TOC [26,27], commensurate reduction of fundamental thermal noise in SMF has never been demonstrated. Furthermore, it is not clear whether such approaches, which focus on tuning the low-frequency thermal behavior of the whole fiber to minimize the effect of environmental temperature changes, would also succeed to reduce phase noise induced by fundamental thermal noise at the higher frequencies where this contribution can be dominant.

Recently, interest in fundamental thermal noise minimization has been renewed by the emergence of new optical fibers that guide the light through a central hole, hollow-core fibers (HCF), which are now surpassing conventional solid glass-core SMF in almost all key properties. Critically, several HCF designs now display propagation loss close to or even below that of the best SMF and allow effective single-mode operation (i.e., the loss of the higher-order modes is significantly higher than that of the fundamental mode), making them suitable in a host of interferometric applications [28]. Hollow-core fibers have already been shown to be less temperature sensitive than conventional SMF [1,2,29,30], a property related to the weak interaction of the mode field with the glass microstructure in addition to the relatively low TOC of the internal gas medium (which promises improvements with core evacuation [31]). Clearly, this low sensitivity to temperature should translate to a weak conversion of thermodynamic temperature fluctuations to path-length fluctuations, as suggested by a first experiment with short, early-design commercial HCFs at the limit of measurement noise [32]. Yet, a model of HCF fundamental thermal noise that goes beyond a simple scaling of the SMF model is still lacking, and measurements at a sufficient dynamic range to reveal its most important properties have never been performed.

In this work, we study fundamental thermal noise in the latest generation of hollow-core fibers [33], which guide light using an antiresonant reflection mechanism (or inhibited coupling [34]). We first review the model of fundamental thermal noise that is usually adequate for SMF above 1 kHz, giving simplified expressions which expose the important design parameters. We then explain how we adapt this model to the case of an antiresonant HCF, stating our main working hypotheses. With a carefully designed characterization setup supporting an order of magnitude more power than what is usually achieved, and using two long-length nested antiresonant nodeless fibers (NANFs [28], 219 m), we measure fundamental thermal noise in the 20 to 200 kHz range with large dynamic range and show that its spectrum agrees with the simple model presented here, at least at room temperature and for internal gas pressures in the 0.1 to 1 atm range. In particular, the noise reduction associated to partial core evacuation indicates that

this fundamental noise, under such experimental conditions, is driven by the thermo-optic contribution of the gas that fills the core, which constitutes a fundamental hypothesis of our model. Extrapolating our results, we finally discuss a potential approach to minimize fundamental thermal noise in HCFs beyond the demonstrated core evacuation.

II. THEORY

A. Solid-core fiber

A fundamental result of thermodynamics [35] is that a system in thermal equilibrium with a heat reservoir, such as an optical fiber or any waveguide held at a constant temperature T, displays fluctuations of its internal energy $u(t)$, where t is the time variable. Although by definition the temperature itself does not fluctuate, it is convenient to define an "effective" or "apparent" temperature representative of the volumetric energy fluctuations, $\Delta T(t) \equiv \Delta u(t)/c_v$, where $\Delta u(t)$ denotes the fluctuations of $u(t)$ about the equilibrium value $\langle u(t) \rangle$ while c_v is the isochoric volumetric heat capacity of the system [3]. The apparent temperature fluctuations are local and can be seen to be the result of random exchanges of energy between neighboring domains of the system, which still globally obeys the law of conservation of energy [36]. From the point of view of an optical mode, the variance of the apparent temperature noise $T_m(t)$, which is spatially averaged over the mode volume V_m, is given by the simple expression

$$\langle \Delta T_m^2(t) \rangle = \frac{k_B T^2}{V_m c_v}, \tag{1}$$

where k_B is the Boltzmann constant [3]. For the fundamental mode in a fiber, it is usually adequate to define $V_m = A_m L = \pi a^2 L$, where A_m is the effective mode area [37], L is the physical fiber length, and a is the equivalent Gaussian mode radius (e^{-2}).

By solving the heat equation with a Langevin source [16], or alternatively by computing the thermal admittance function and invoking the fluctuation-dissipation theorem [38], it can be shown that the one-sided power spectral density (PSD) of the apparent temperature fluctuations takes the following general form:

$$S_{\Delta T_m}^{(1)}(f) = \langle \Delta T_m^2(t) \rangle Q(f), \tag{2}$$

where $Q(f)$ is a spectral shape function which depends on the thermal boundary conditions, thermal properties of the material, and mode-field area, and where f is the frequency variable. For a very large, thermally uniform fiber ("infinite" boundary conditions, neglecting the potential impact of index-raising dopants over the thermal properties), $Q(f)$ has unit area and can be simplified as

$$Q(f) = \frac{2}{\pi f_c} \text{Re}[e^{jf/f_c} E_1(jf/f_c)], \tag{3a}$$

$$\int_0^\infty Q(f) df = 1, \tag{3b}$$

where $\text{Re} = [\cdot]$ denotes the real part, j is the imaginary unit, and E_1 is the exponential integral function. Although this expression is different from those found in [16,38], it is ultimately equivalent but has the advantage of clearly separating the variance term (total power or PSD area) from the spectral shape which is only parametrized through f_c, a cutoff
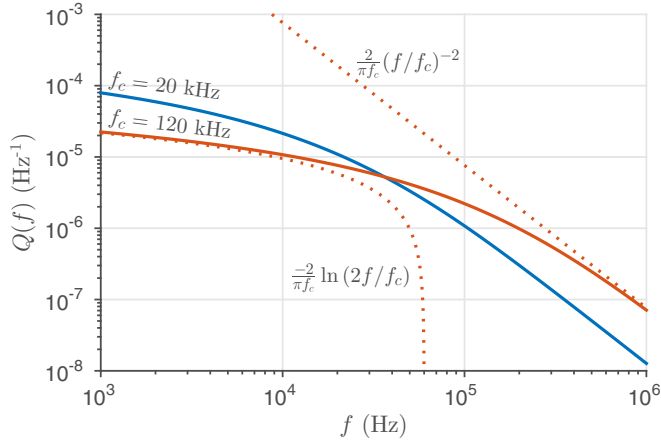
FIG. 1. Spectral shape function for the case of infinite boundary conditions; comparison of two cutoff frequencies. Low-frequency and high-frequency asymptotes are shown in dotted orange for $f_c = 120$ kHz.

frequency defined as

$$f_c = \frac{2k_t}{A_m c_v},\tag{4}$$

where k_t and c_v are the thermal conductivity and heat capacity of the fiber material, respectively. In a typical SMF operated around 1550 nm, $f_c \approx 20$ kHz, giving the shape function illustrated in blue (uppermost at low frequencies) in Fig. 1. Since $Q(f)$ has unit area, a larger cutoff frequency simply means that the noise power of Eq. (1) is spread over a larger bandwidth, lowering the low-frequency PSD level. In silica SMF, such an increase of the cutoff frequency can be achieved through reduction of the mode area (e.g., by decreasing the operating wavelength or decreasing the core diameter under certain conditions), as illustrated in orange (lowermost at low frequencies) in Fig. 1 for a case where the effective mode radius is 2.45 times smaller than that of a typical SMF.

When other, more realistic thermal boundary conditions are assumed, the spectral shape function $Q(f)$ takes a different form which is less insightful and does not necessarily maintain a unit area [16]. However, Eq. (3a) still accurately describes the spectrum of high-frequency temperature fluctuations. Indeed, the cutoff frequency f_c can be seen to be a ratio of thermal diffusivity to mode area; it is associated to the averaging of temperature fluctuations, which are correlated in time and space because of thermal conduction, over the mode cross-sectional area. It is thus useful to define the frequency-dependent thermal correlation length:

$$l_t(f) = \sqrt{\frac{k_t}{2\pi c_v f}} = \frac{a}{2}(f/f_c)^{-1/2}.\tag{5}$$

At those frequencies for which $l_t(f)$ is a few times smaller than the cladding radius, it is appropriate to ignore the exact form of the boundary conditions and thus use the simple form of $Q(f)$, valid for an infinite cladding. In SMF, this condition is true above approximately 100 Hz.

To relate the apparent temperature fluctuations $\Delta T_m(t)$ to phase fluctuations $\phi(t)$ which can be measured interferometri-

cally, it is usually assumed that the optical length at any instant is directly related to the apparent temperature [4,16,38]:

$$\phi(t) = \frac{2\pi}{\lambda}\frac{d(nL)}{dT}\Delta T_m(t) = \frac{2\pi nL\xi}{\lambda}\Delta T_m(t),\tag{6a}$$

$$\xi \equiv \alpha_L + \frac{1}{n}\frac{dn}{dT},\tag{6b}$$

where n is the effective index of the fundamental guided mode, λ is the vacuum wavelength, α_L is the thermal expansion coefficient (TEC), dn/dT is the thermo-optic coefficient for the effective index (or "effective TOC"), and ξ is the temperature sensitivity. If this relation holds, the phase fluctuations PSD is given by

$$S_\phi^{(1)}(f) = \left(\frac{2\pi nL\xi}{\lambda}\right)^2 S_{\Delta T_m}^{(1)}(f),\tag{7}$$

which is the main result of this section. The noise described by Eqs. (1), (2), and (7) has been called "thermoconductive" by Foster [16] and it is qualitatively similar to the noise previously described by Wanser [4]. It is also similar to thermorefractive noise measured in microcavities [39] and dielectric mirrors [40] when the TEC is much smaller than the TOC, as is the case in fused silica. It is, however, distinct from thermomechanical noise driven by internal damping [38], akin to Brownian noise in ultrastable cavities [41], which is predicted to be important in the sub-kHz spectral range only [42] and whose theoretical description is not entirely supported by experimental data [43]. Since our experimental demonstration is centered on the 20 to 200 kHz range, we ignore thermomechanical noise in this paper. Note that because the temperature noise PSD is proportional to $1/L$ [Eq. (2)], the phase noise PSD of Eq. (7) is proportional to L and not L^2; this expresses the fact that the total optical path-length fluctuation is given by the incoherent sum of all optical path-length fluctuations along the fiber length (i.e., any longitudinal spatial correlation is short ranged).

To model thermoconductive phase noise, we choose to use physical values representative of the material close to the mode field, that is, within a few thermal correlation lengths of the fiber axis. We thus completely ignore the potential contributions of the fiber coating and jacket. Although these do matter at low frequencies [18,44], we heuristically argue that these should not contribute to the apparent temperature noise sampled by the mode field above a few kHz. Furthermore, since our experimental demonstration is based on a polarization-maintaining single-mode fiber (PM-SMF) of PANDA configuration, we use values tabulated in [45] for the slow axis of a PANDA fiber; in addition to the dominant thermo-optic coefficient of the core and cladding material, these take into account the impact of geometry deformation and stress-optical effect over the effective index n, yielding $n^{-1}dn/dT = 6.10$ ppm/K. The contribution of the boron stress-applying parts to the TEC is also considered, yielding $\alpha_L = 1.05$ ppm/K for a naked fiber and presumably also for the material close to the core. Overall, the sensitivity of the PM-SMF is thus $\xi \approx 7.15$ ppm/K, which is comparable to the values used in standard SMF-28 for the purpose of thermoconductive noise modeling around 1550 nm [3,16,38,43,46]. All physical parameters used in this paper for SMF are summarized in Table I.

TABLE I. SMF parameters used in the thermoconductive noise model [16,45].

Symbol	Name	Value
c_v	Volumetric heat capacity[a]	1.67×10^6 J m^{-3} K^{-1}
k_t	Thermal conductivity	1.37 W m^{-1} K^{-1}
a	Mode-field radius (e^{-2})	5.25×10^{-6} m
n	Effective index	1.45
dn/dT	Thermo-optic coefficient	8.84×10^{-6} K^{-1}
α_L	Thermal expansion coefficient	1.05×10^{-6} K^{-1}

[a]At constant volume.

B. Gas-filled hollow-core fiber

The thermoconductive noise model has been explicitly developed (by other authors) for solid-core fibers, and here we only considered the effect of the material close to the core region to describe the noise at high frequencies. In this work, we suppose that the same model still adequately describes thermal noise in gas-filled antiresonant hollow-core fibers, heuristically replacing the glass core by a gas core with suitable thermo-optic and thermal properties. To this end, we make a series of simplifying assumptions; these are later shown to adequately explain phase noise measured in antiresonant HCFs above 20 kHz. First, we consider only the fundamental mode and neglect the contribution the microstructure may have over the thermal properties. Basing the model on the properties of the gas that resides in the core cavity is especially justified in antiresonant HCF for which the fraction of power guided in glass is 10^{-4} or lower [28]. Second, we suppose that thermal expansion is negligible ($\alpha_L \approx 0$), following our reasoning that material far from the fiber axis (in this case the silica cladding, that is, the tube which supports the microstructure) should not significantly contribute to phase noise at high frequencies. This also implies we neglect the small structural deformation (microstructure, cladding, end faces) associated to fluctuations of the gas' apparent temperature in addition to the impact of thermal boundary conditions. Third, we neglect convective effects, which should be much slower than conduction and should only manifest at low frequencies [47]. Finally, to keep the model simple and to expose the main trends, we assume the hollow core is filled with nitrogen (N$_2$) at a pressure such that the Knudsen number Kn, defined as the ratio of mean-free path to capillary diameter, stays below 0.01. This constitutes the condition to remain in the hydrodynamic flow regime [48]. For the HCF used in our experimental demonstration, this condition is respected for an internal pressure above 0.2 atm (20 kPa), approximately, if the capillary diameter is taken to be similar to the core diameter (35 μm). While the gas inside a typical hollow-core fiber is better described as a mixture of molecules with exact partial pressures dependent on the fabrication procedure and handling history, it should be safe to assume that nitrogen is the dominant species under most conditions; the error introduced by the presence of atmospheric constituents (O$_2$, CO$_2$, etc.) is predicted to be relatively small since the thermal and optical properties of air at standard temperature and pressure (STP) are very similar to those of nitrogen [$c_v = 855$ J/(m^3 K) and $k_t = 0.026$ W/(m K) [49],

$dn/dT = 910$ ppb/K [50]]. The same reasoning applies to argon which is often used as pressurization gas during fabrication (see Sec. IV).

Given the simplifications made here, only the thermal (c_v, k_t) and thermo-optic (dn/dT) properties of the gas that fills the hollow core are required to describe fundamental thermal noise in HCF [in antiresonant HCFs, the fundamental mode's effective index n is a few hundreds of ppm smaller than unity [51]; it is hence adequate to simply set $n = 1$ in Eq. (7)]. First, the volumetric heat capacity of diatomic molecules can be expressed as

$$c_v = \frac{5p}{2T}, \tag{8}$$

where p is the pressure [52]. This evaluates to $c_v = 860$ J/(m^3 K) at STP. The thermal conductivity, on the other hand, is independent of pressure in the hydrodynamic flow regime and has a value of approximately 25.4 mW/(m K) in N$_2$ at 20 °C [53]. Taking the mode area of SMF, this means that the cutoff frequency [Eq. (4)] is 670 kHz in nitrogen gas, 35 times larger than it is in silica, spreading the total noise power over a much wider bandwidth. In our demonstration, however, the mode-field radius of the HCF is 12.5 μm, much larger than in SMF, yielding $f_c \approx 120$ kHz as shown in orange (lowermost at low frequencies) in Fig. 1. Finally, to estimate the thermo-optic coefficient dn/dT required to model ξ [Eq. (6b)], we describe the index of the gas within the core n_c using the Lorentz-Lorenz equation [54]

$$\frac{n_c^2 - 1}{n_c^2 + 2} = \frac{4\pi\alpha N}{3} \approx \frac{2}{3}(n_c - 1), \tag{9}$$

where α is the molecular polarizability volume (not to be confused with the TEC α_L), N is the number density, and the last approximation is valid if $n_c \approx 1$, which is the case for gases at ordinary densities. The thermo-optic coefficient of a gas obeying this equation can be found through differentiation of n_c:

$$\frac{dn_c}{dT} \approx 2\pi \left(\frac{d\alpha}{dT} N + \alpha \frac{dN}{dT} \right). \tag{10}$$

The factor dN/dT would normally be assumed to be zero in a sealed hollow-core fiber [31] since the number of gas molecules is constant and since we ignore fluctuations of the internal volume, making the number density invariant. The ideal gas law can be used to write $N = p/(k_B T)$, and the corollary is that the pressure is normally assumed to be directly proportional to temperature. However, the thermo-optic coefficient used in the noise model relates to *local* apparent temperature fluctuations. The assumption here is that if locally the temperature fluctuates, the pressure is still constant in the vicinity of the fluctuation and therefore the local density also fluctuates ($dN/dT \neq 0$) according to the gas law, leading to a phase fluctuation in the propagating light. Note that these density fluctuations should be uncorrelated along the fiber length, at least at those frequencies much larger than the ratio of acoustic velocity to fiber length, provided that the fiber mode does not fill the entirety of the hollow core such that gas molecules have the possibility of moving in and out of the guided mode. The thermo-optic coefficient should thus be computed assuming constant local pressure ($dp/dT = 0$)

TABLE II. HCF parameters used in the thermoconductive noise model.

Symbol	Name	Value
c_v	Volumetric heat capacity[a]	$860\left(\frac{p}{p_0}\right)$ J m^{-3} K^{-1}
k_t	Thermal conductivity[b]	0.025 W m^{-1} K^{-1}
a	Mode-field radius (e^{-2})	12.5×10^{-6} m
n	Effective index	1.00
dn/dT	Thermo-optic coefficient	$936 \times 10^{-9}\left(\frac{p}{p_0}\right)$ K^{-1}

[a]At constant volume.

[b]Kn < 0.01.

instead of constant volume ($p \propto T$), even if the fiber is sealed. This agrees with the models used in photothermal interferometry, which have been developed and successfully compared with experimental data over a frequency range similar to that of interest here [55–58]. Under this perspective, we can rewrite Eq. (10) using $dN/dT = -p/(k_B T^2)$ (constant pressure):

$$\frac{dn_c}{dT} \approx \frac{2\pi p}{k_B T}\left(\frac{d\alpha}{dT} - \frac{\alpha}{T}\right). \qquad (11)$$

The second term within parentheses is typically much larger than the first one; for example, in N$_2$ at STP, $\frac{d\alpha}{dT} = 1.85 \times 10^{-36}$ m^3/K while $\frac{\alpha}{T} = 5.95 \times 10^{-33}$ m^3/K [59]. We can thus simplify

$$\frac{dn_c}{dT} \approx -\frac{2\pi p\alpha}{k_B T^2}, \qquad (12)$$

which gives $\xi \approx -936$ ppb/K when combining all our hypotheses, critically that $dn/dT \approx dn_c/dT$. The parameters of the HCF used in our demonstration, at a temperature $T = 20\,°$C, are summarized in Table II; this includes the pressure dependence when appropriate ($p_0 = 101.3$ kPa $= 1$ atm).

To compare the fundamental thermal noise in fibers having distinct lengths and indices, the phase PSD can be normalized by the optical length nL, yielding

$$\frac{S_\phi^{(1)}(f)}{nL} = n\left(\frac{2\pi\xi}{\lambda}\right)^2 \frac{k_B T^2}{A_m c_v} Q(f). \qquad (13)$$

Although another normalization could certainly be chosen, this one is justified by the fact that the signal of interest scales with the optical instead of physical length in most applications. Furthermore, it gives a quantity that is independent of physical length, which is not the case of the signal-to-noise ratio (SNR) which increases with it. From this normalized phase PSD, and assuming the same wavelength, mode area, and temperature, it is apparent that a HCF filled with nitrogen at STP displays a much larger temperature variance than a SMF because its heat capacity is lower by more than two orders of magnitude. This is partially compensated by a higher cutoff frequency, which spreads the noise over a larger bandwidth [through $Q(f)$], and a weaker conversion of temperature to optical length (through ξ). Finally, for equal optical lengths, the mode volume is larger in a gas than in a transparent solid since the effective index is close to unity; this explains the remaining factor n in the right-hand side of Eq. (13).
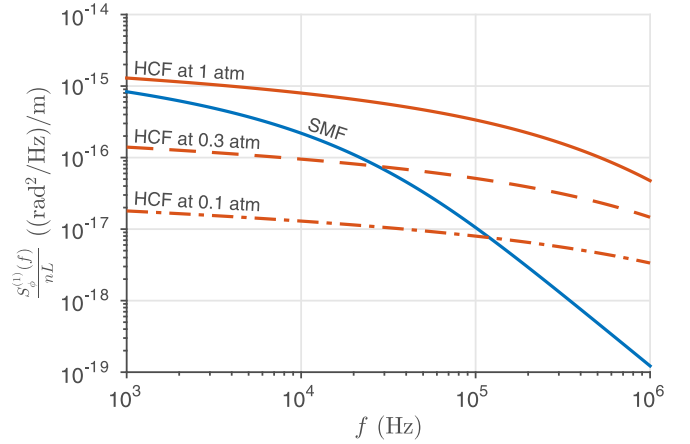

FIG. 2. Modeled optical-length-normalized phase PSD at $\lambda = 1539.8$ nm. Comparison between SMF and HCF filled with N$_2$ at three different pressures. The parameters are $T = 20\,°$C and $a = 5.25\,\mu$m (SMF and HCF have the same mode-field area, in contrast to the figures shown in Sec. III).

The SMF to HCF comparison is quite different if the HCF's pressure is assumed to be lower than 1 atm, as shown in Fig. 2, mostly because the detrimental impact of a reduced heat capacity is largely compensated by the higher cutoff frequency and lower TOC. Let us suppose here that we are interested in frequencies below the cutoff f_c so that Eq. (3a) can be replaced by its low-frequency asymptote:

$$Q(f)|_{f \ll f_c} \approx \frac{-2}{\pi f_c}\ln\left(\frac{2f}{f_c}\right). \qquad (14)$$

Neglecting the weak logarithmic dependence, this expression shows that the spectral shape function at low frequencies is roughly proportional to f_c^{-1} or c_v/k_t. For pressures such that Kn < 0.01, the thermal conductivity is pressure independent and the phase noise PSD at low frequencies is therefore proportional to p^2 because $\xi \propto p$, as suggested by the orange curves in Fig. 2. Considerable noise reduction should thus be possible with core evacuation. However, it is worth stating that other fundamental noise sources can start to dominate the spectrum at low and high frequencies if the thermoconductive noise contribution is lowered. Ultimately, a more accurate and detailed model able to address this point could be obtained through finite-element simulation [41].

III. EXPERIMENT

The fundamental thermal noise of several fiber samples was measured by comparing pairs of unbalanced Mach-Zehnder interferometers illuminated by the same laser signal. The advantage of this approach is that laser noise, which is usually much larger than fundamental thermal noise, is common to both interferometric phase outputs and can be canceled through subtraction. This subtraction can then be tuned in postprocessing to account for unequal interferometric lengths and laser noise gains. Traditionally, this would instead be achieved using a balanced fiber interferometer, with laser noise rejection highly dependent on the fine adjustment of the arm lengths. Subtracting the two phase signals also
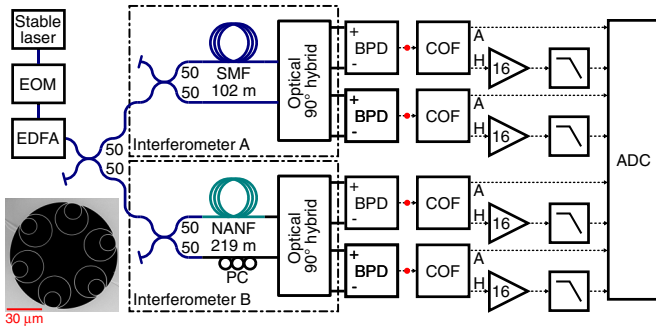
FIG. 3. Layout of the experimental setup showing a comparative measurement between interferometer A (in this case SMF) and B (in this case HCF or NANF). The dashed boxes can be switched for SMF to SMF comparison or HCF to HCF comparison. EOM, electro-optic phase modulator; EDFA, erbium-doped fiber amplifier; PC, polarization controller; BPD, balanced photodetector; COF, crossover filter ("A" stands for "attenuated," "H" stand for "high-pass"); ADC, analog-to-digital converter (digitizer). Solid lines represent fibers (all fibers are polarization maintaining except in a HCF interferometer) and dashed lines represent electrical cables. The dots between BPD and COF indicate the points where the synthesizer is connected for frequency response precharacterization. The inset shows a scanning electron micrograph of the HCF's cross section.

suppresses environmental fluctuations that are partially correlated between the interferometers and, critically, exposes the independent thermal noise contributions that are of interest here. In this section, we first give information about the instrumentation we developed and the fiber samples we manufactured, explaining the tradeoffs associated to thermoconductive noise measurement. We then briefly describe the signal-processing approach before presenting the main results.

A. Instrumentation

The experimental setup in which two fiber samples are used is illustrated in Fig. 3. For clarity, we show the specific case of a SMF to HCF comparison, but all possible fiber combinations (SMF-SMF, HCF-HCF, SMF-HCF) are studied below. The laser is an OEwaves WGM Gen3 with 195-THz mean frequency (λ = 1539.8 nm) and 7-mW output power. It is amplified using a custom-made, polarization-maintaining erbium-doped fiber amplifier so that the optical power at the input of each interferometer is approximately 10 mW. The laser can be frequency modulated (internally) and phase modulated (externally, using an EOSpace PM-085-20-PFA-PFA-1550) for signal-processing purposes described below.

After recombination using optical 90° hybrids (Kylia COH24 for SMFs and Optoplex HB-T0AFAS001-R1 for HCFs), the interferometric signals are routed to four custom-made balanced photodetectors (Thorlabs FGA01FC photodiodes) with 2000-Ω transimpedance gain, 0.8 quantum efficiency, 10-MHz bandwidth, and a 17-V saturation level sufficient to handle the maximum possible power per photodiode (5 mW). In order to maintain a high dynamic range, custom-made crossover filters (COF) are used to separate the ac and dc parts of each signal. Each ac signal, carrying the phase-noise information, is amplified using an EG&G 5113 preamplifier (16 V/V, 300 Hz to 1 MHz), filtered by a

500-kHz antialiasing filter (Thorlabs EF506 low-pass electrical filter), and finally digitized using a GaGe CSE8389 digitizer set in the voltage range that provides the best dynamic range (±2 V for a noise level of approximately 2×10^{-12} V^2/Hz below a 50-kHz resonance, and 5×10^{-13} V^2/Hz above it). For this setup, digitizer noise is dominant over detector noise and preamplifier noise, but significantly weaker than shot noise. Each dc signal, carrying the information about the fringe position, is attenuated by 20 dB in the COF to prevent damage to the digitizer. The four ac signals and four dc signals are simultaneously sampled at a rate of 10 MS/s for a total duration of 0.4 s.

B. Fiber samples

Two PM-SMFs (Fujikura SM15-PS-U25A, PANDA, hereafter referred to as SMFs) with nominal length $L = 102$ m and mode-field radius $a = 5.25\ \mu$m were used for this demonstration (other relevant properties are shown in Table I). Each fiber was spooled in a single layer on the surface of an aluminum cylinder of diameter 10.2 cm and height 7.6 cm. We did not attempt to minimize the length of the couplers' pigtails that contribute to the path imbalance, which we measured to be 3 m in total (the relevant length for fundamental thermal noise computation is 105 m while the length relevant for laser noise conversion is 102 m). Similarly, two antiresonant HCF samples (NANF) with nominal length $L = 219$ m and mode-field radius $a = 12.5\ \mu$m were used (Table II). These fibers were fabricated using the same stack, fuse, and two-stage draw process reported in [33]. They were drawn to a core diameter of approximately 35 μm and average cladding membrane thickness of 550 nm and their loss was measured via cutback to be 1.3 dB/km at our operating wavelength. Note that effective single-mode propagation can be assumed for such a length of NANF [28,33]. One HCF sample was spooled on an aluminum cylinder similar to those used for the SMFs (diameter 12.6 cm, height 12.7 cm) and the other HCF was loosely spun on a standard plastic shipping spool. The total length of the SMF pigtails contributing to the path imbalance was estimated to be 4.5 m in both cases. Additional information about these HCFs, including details about the HCF to SMF interconnections, can be found in [60].

C. Fiber length optimization

The total phase noise measured by an interferometer based on a 90° hybrid output coupler, hereafter referred to as an IQ interferometer (for "in-phase and quadrature"), which is adjusted to introduce a negligible delay in one arm and a phase delay $\tau = nL/c$ in the other arm, can be modeled as

$$\theta(t, \tau) = \nu(t) * g(t, \tau) + \phi(t, \tau) + \epsilon(t, \tau) + \mu(t, \tau), \quad (15)$$

where $\nu(t)$ is the frequency noise of the laser illuminating the interferometer, $*$ is the convolution operator, $g(t, \tau) = 2\pi \Pi(t/\tau - 1/2)$ is the impulse response describing the conceptual filter that converts laser frequency into interferometric phase, with Π as the unit-width boxcar function [61], $\phi(t, \tau)$ is the phase noise induced by fundamental thermal noise as defined in Sec. II, $\epsilon(t, \tau)$ is the phase noise induced by environmental noise (vibrations, temperature drift, etc.), and $\mu(t, \tau)$ is the measurement noise contribution that
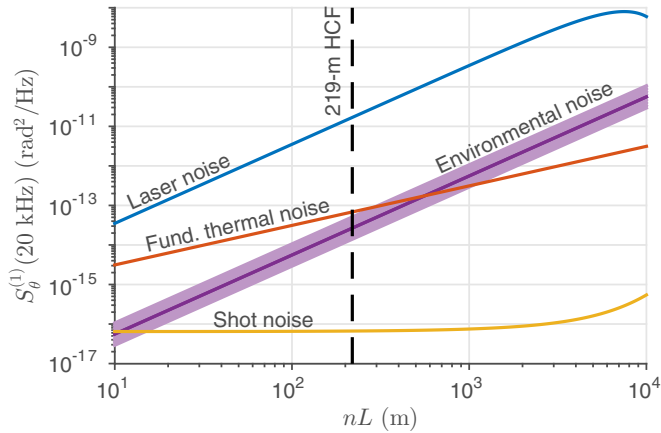
FIG. 4. Modeled contributions to the total phase noise PSD at 20 kHz [see Eq. (15) and definitions in the paragraph that follows]. The laser noise curve (top) assumes $S_\nu^{(1)}(20 \text{ kHz}) = 0.8 \text{ Hz}^2/\text{Hz}$ and shows a cutoff due to bandwidth reduction with increase in nL, the fundamental thermal noise (mid) is based on Eq. (7) for an antiresonant HCF at 1 atm internal pressure, and the measurement noise curve (bottom) supposes that shot noise is dominant with $P_0 = 10$ mW, $\eta = 0.8$, and a fiber transmission loss of 1.3 dB/km. Environmental noise (mid, shaded) is traced as a possible distribution to illustrate the typical trend with increasing fiber length; in practice, it can take vastly different values depending on the exact environmental conditions and the interferometer's environmental sensitivity.

is converted to phase. Figure 4 illustrates phase contributions that roughly replicate our experimental conditions at 20 kHz. When shot noise is dominant, the PSD of $\mu(t, \tau)$ is white with level $S_\mu^{(1)}(f) = 2h\nu_0[1 + \gamma(\tau)^{-1}]/(\eta P_0)$, where h is the Planck constant, $\nu_0 = c/\lambda$ is the laser mean frequency, $\gamma(\tau)$ is the transmittance of the delay arm, η is the photodetector's quantum efficiency, and P_0 is the optical power measured at the input of the interferometer [62]. From the Fourier transform of $g(t, \tau)$, the phase-noise PSD associated to converted laser frequency noise can be expressed as $[2\pi\tau\,\text{sinc}(f\tau)]^2 S_\nu^{(1)}(f)$. The bandwidth of the laser noise contribution therefore diminishes with increasing path imbalance while its low-frequency gain increases. Furthermore, the PSD of $\epsilon(t, \tau)$ is usually proportional to τ^2 since environmental perturbations tend to affect the whole fiber in a coherent fashion. Changing the phase delay τ, i.e., changing the path imbalance or fiber length, therefore changes the PSD level of the four independent noise signals.

From Eq. (15) and Fig. 4, two simple conclusions can be drawn. First, a minimum fiber length is required to bring fundamental thermal noise above shot noise, and this minimum length ultimately depends on the maximum power which can be handled by the fiber components and photodetectors (and also on the finesse if a resonator configuration is used [63]). In Fig. 4, given the input power and thermal noise model, this minimum length is $nL \approx 0.2$ m at 20 kHz, but it would increase to 0.9 m at 120 kHz and 6.5 m at 500 kHz. Second, increasing the fiber length raises laser noise and environmental noise much faster than it does fundamental thermal noise; longer unbalanced interferometers are therefore more difficult to stabilize and require strong laser noise suppression, extreme

laser stability, or both. For this demonstration, we assembled 219-m HCF samples (nL) since we calculated that laser noise suppression would be sufficient (given the frequency noise of the laser we used) for such an optical length and since our goal was to expose fundamental thermal noise at high frequencies with a large dynamic range. However, and as detailed below, we found out that environmental noise, which is much more difficult to model before the fact, constitutes the limitation of our measurements below approximately 20 kHz. To expose fundamental thermal noise in this acoustic frequency range, shorter interferometers would be preferable since they are less sensitive to thermal drift and vibrations (which tend to be much stronger at low frequencies), though this comes at the expense of a reduced shot-noise-limited signal-to-noise ratio and commensurate lower measurement bandwidth. Ultimately, the fiber length that is optimal to expose fundamental thermal noise depends on the exact experimental conditions, in particular environmental fluctuations, and is necessarily frequency dependent.

D. Signal processing

A series of precharacterizations of the setup were first performed. Using an amplitude-modulated laser to directly illuminate each of the eight photodiodes, the frequency responses $H_d(f)$ were measured in order to guarantee adequate bandwidth and common-mode rejection [Fig. 5(a)]. Similarly, a synthesizer was connected at the input of the crossover filters for the measurement of the frequency response $H_f(f)$ in both the ac and dc branches [Fig. 5(b)]. Finally, with the setup configured as in Fig. 3, the laser was frequency modulated with approximate peak-peak amplitude $\Delta\nu = 1/(500 \text{ ns}) = 2$ MHz in order to trace a complete interferometric fringe [Fig. 5(d)]. This allowed the extraction of the IQ parameters of the optical 90° hybrids through an elliptic fit [62]. Final measurements were taken with the frequency modulation turned off, and the dc and ac signals [see an example in Fig. 5(c)] were both digitally equalized to compensate the appropriate frequency response, low-pass filtered at 500 kHz (a frequency beyond which the frequency response inversion is difficult because of the antialiasing filter rolloff), recombined digitally, and then corrected for ellipticity. From the fully corrected composite IQ signals, the total phase noise $\theta(t)$ could be extracted unambiguously, regardless of the operating phase (fringe position) [64]. Similarly, synthetic measurement noise signals could be constructed by instead using ac noise signals acquired with the laser turned off. We found that the complete precharacterization procedure only had to be performed every hour to maintain adequate accuracy, mostly due to the slow drifts in polarization in the HCF interferometers.

As suggested in Fig. 4, laser noise is largely dominant in the output phase of each interferometer, even if a highly stable laser is used. To suppress as much of this noise as possible, the laser signal was phase modulated following a triangle waveform so as to create a pilot signal (in this case a square wave) in the output phase. This pilot signal was then used to estimate the difference in phase delay between both interferometers. From the complex ratio of the harmonics found in each output spectrum, a correction function of the
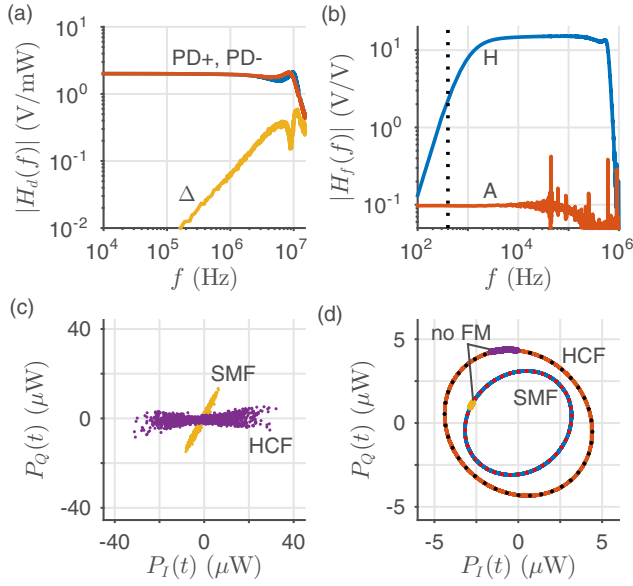
FIG. 5. Typical responses and signals. (a) Photodetector circuit frequency responses (modulus). "PD+" and "PD−" stand for positive and negative photodiode channels, respectively, while "Δ" refers to the modulus of the difference, an indicator of the common-mode rejection level. (b) Crossover filter frequency response (modulus). "A" stands for "attenuated" (dc part), "H" stands for "high pass" (ac part). The dotted black line marks the transition frequency. (c) Corrected and calibrated ac signals for both interferometers (0.4-s duration). The larger excursions observed in HCF are due to a stronger laser noise conversion (due to the larger path imbalance) and stronger acoustic noise pickup. (d) IQ ellipses for the case illustrated in Fig. 3. The dotted lines are the associated elliptical fits. Also shown are the corrected and calibrated composite signals (no FM) which are the complement to those shown in (c); no laser frequency modulation (FM) is applied in these cases.

following form was computed:

$$H_c(f) = \frac{1 - e^{-j2\pi f \tau_A}}{1 - e^{-j2\pi f \tau_B}} \approx \frac{\tau_A}{\tau_B} e^{-j\pi f(\tau_A - \tau_B)}, \quad (16)$$

where τ_A (τ_B) is the phase delay in interferometer A (B) and the approximation is adequate for the conditions of interest here. Constructing a corrected phase difference of the form $\Delta\theta'(t) = \theta_A(t) - \theta_B(t) * h_c(t)$, where $h_c(t)$ is the impulse response associated to $H_c(f)$ and θ_A (θ_B) is the total phase from interferometer A (B) [see Eq. (15)], instead of $\Delta\theta(t) = \theta_A(t) - \theta_B(t)$ improves laser noise suppression; this improvement is shown in Fig. 6(a) for the case of a SMF to SMF comparison (interferometers A and B are made of SMF), in which the delays are nearly identical ($\tau_A/\tau_B \approx 0.996$), and in Fig. 6(c) for the case of a SMF to HCF comparison, in which the delays are more distinct ($\tau_A/\tau_B \approx 0.705$). Obviously, such a correction scales all terms that contribute to the phase measured in interferometer B [see Eq. (15)], in particular the fundamental thermal noise that is of interest here. However, recognizing that this noise is independent in both interferometers and assuming that it is dominant over environmental noise and measurement noise (which is the criterion for the thermal noise measurement to be valid), it
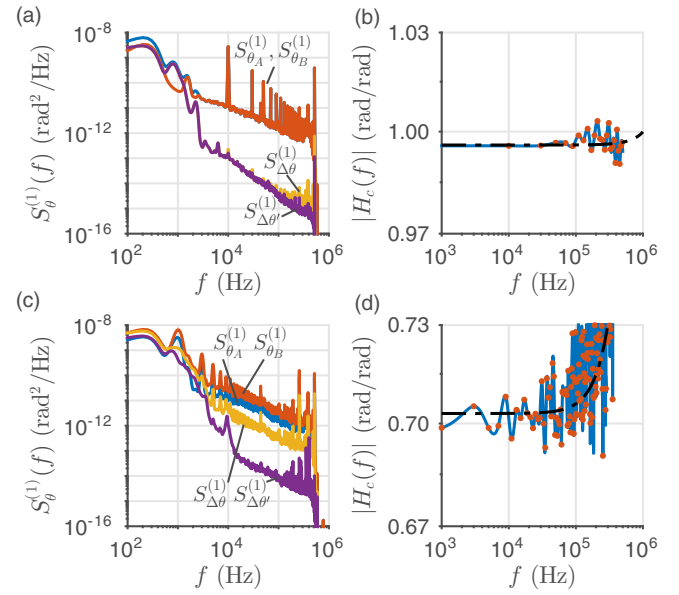

FIG. 6. Improved laser noise suppression using a periodic pilot signal. In (a), the two overlapped curves (top) represent the noise spectrum measured for each interferometer, with harmonics of 10 kHz clearly visible. The two curves at the bottom represent the PSD of the phase difference, without and with delay correction. A slight improvement is visible at high frequencies. The modulus of the correction function is shown in (b) along with the fit (dashed black). The signal-to-noise ratio quickly decreases above 100 kHz and is below 1 above 500 kHz (not displayed). (c), (d) Show an example of the same correction for a SMF to HCF comparison. In this case the pilot signal's frequency is 1 kHz and the suppression improvement is striking since the path imbalances are very different.

is straightforward to take this scaling into account during analysis. Indeed, the PSD of the corrected phase difference simply becomes

$$S_{\Delta\theta'}^{(1)}(f) = S_{\phi_A}^{(1)}(f) + |H_c(f)|^2 S_{\phi_B}^{(1)}(f)$$

$$\approx S_{\phi_A}^{(1)}(f) + \left(\frac{\tau_A}{\tau_B}\right)^2 S_{\phi_B}^{(1)}(f). \quad (17)$$

The measurement noise scales in the same fashion since it is also independent in both interferometers. It is worth stating that this last equation is strictly valid only if the delay in each reference arm is null. Because of pigtails, this is not true in practice, but small corrections can be brought to Eq. (17) once laser noise is canceled. From the corrected phase difference $\Delta\theta'(t)$, we finally computed phase power spectral densities using Welch's method with 80 nonoverlapping segments, a Kaiser window (shape factor $\beta = 10$), and a zero-padding factor of 4 to lightly smooth the display.

E. Results

We first compared the two SMF interferometers for verification purposes. In Fig. 7, the thermoconductive noise model [Eq. (17) with $\tau_A/\tau_B \approx 0.996$ and the parameters found in Table I] is superimposed on the measured phase difference PSD, showing good agreement between 20 and 200 kHz. Above 200 kHz, the PSD approaches the measurement noise
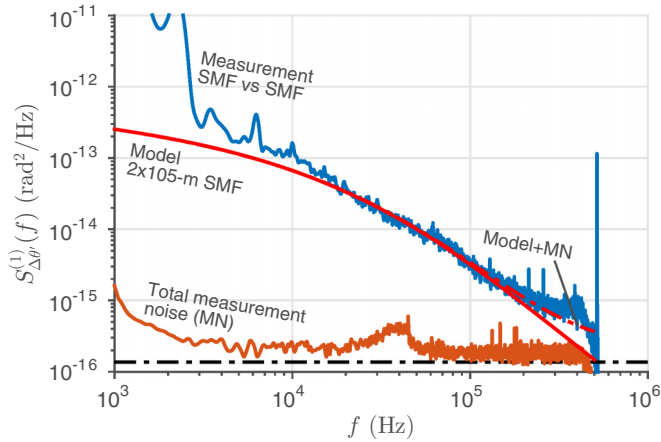
FIG. 7. Difference phase PSD at $\lambda = 1539.8$ nm and $T = 20\,^{\circ}$C, SMF to SMF comparison. The dashed-dotted black curve is the shot noise level $(8.9 + 9.5$ mW).

(MN) floor and then quickly drops off due to the digital low-pass filter. The small hump around 400 kHz is attributed to nonlinear conversion of laser relative intensity noise. At the lowest displayed frequencies, the measurement is limited by building vibration noise, which we confirmed by installing both SMF interferometers on vibration isolation platforms (Minus K, 25BM-10); deactivating the platforms led to a significant increase in the measured phase noise below 3 kHz (the curve shown here is with the platforms activated). Between 3 and 20 kHz, the measured noise is larger than the model by 1 to 2 dB. While it could be tempting to attribute this offset to inadequate modeling of the thermal boundary conditions, the impact of the cladding boundary manifests at lower frequencies in SMF and it tends to decrease the noise level, not increase it [16]. Our hypothesis is that this is again due to vibrations, though of acoustic instead of structural origin. Finally, the measurement noise, shown in orange in Fig. 7, appears dominated by the sum of the two shot-noise contributions ($P_{0,A} = 8.9$ mW and $P_{0,B} = 9.5$ mW), in particular above the 50-kHz noise resonance where the digitizer noise level drops abruptly. This agrees with our measurement noise model.

We then compared the two hollow-core fibers using the same setup (Fig. 8). In this case, we found a much higher vibration contribution below 20 kHz; this is not surprising given the higher intrinsic acoustic sensitivity of HCFs [65] in addition to the fact that we did not shield the HCF interferometers as much as the SMF interferometers in order to facilitate polarization tuning. Between 20 and 200 kHz, we measured a phase PSD that sits within 2 dB of our adapted thermoconductive noise model (Table II), with a spectral shape clearly distinct from that in SMF. However, we found that we could significantly improve the match between measurement and model, in both shape and level, by assuming the internal pressure of both HCFs to be 0.7 atm instead of 1.0 atm. Although it is difficult to corroborate such an observation, recent investigations have shown that the pressure inside a HCF right after fabrication is significantly below 1 atm [66]. Depending on the time a hollow-core fiber is left open to the atmosphere
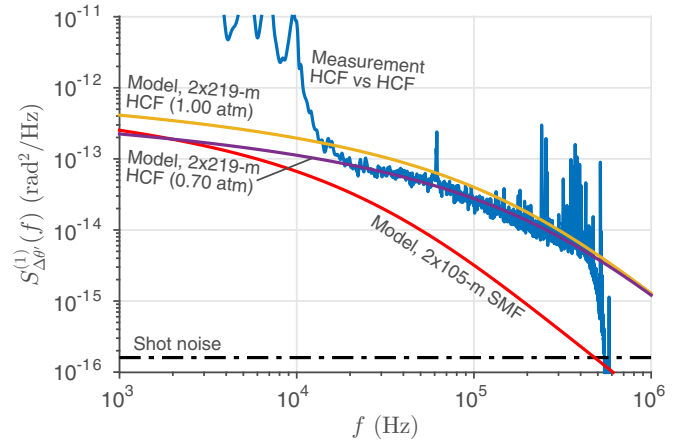
before being sealed, and depending on its total length [48,67], it is possible for the internal pressure to settle to a fraction of atmospheric pressure. While we do not know how long our HCF samples were left unsealed postfabrication, both were cut from adjacent sections of the drawn fiber. Furthermore, we followed the same procedure to build the HCF to SMF interconnections, only breaking the seal at the moment of splicing. It therefore appears reasonable for both samples to display a similar internal pressure of approximately 0.7 atm.

To validate this first thermoconductive noise measurement in HCF, we also compared each of the HCF to the same SMF, in this case applying a strong subtraction correction to better suppress laser noise (Fig. 9). In both cases, we found a good agreement between measurement and model, once again assuming an internal pressure of 0.7 atm for each HCF. The three independent measurements of HCF noise are therefore
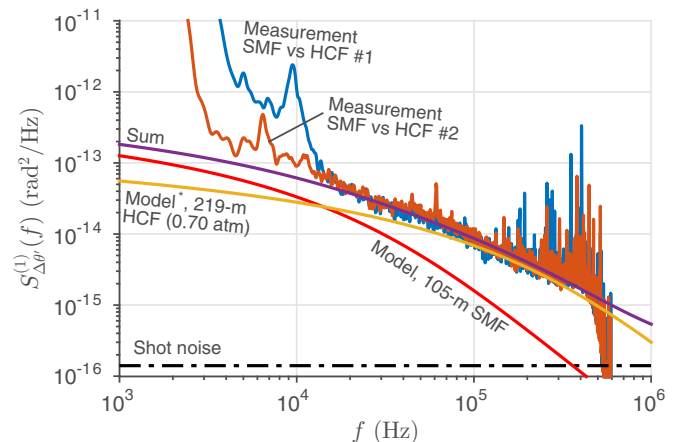

FIG. 8. Difference phase PSD, HCF to HCF comparison (before evacuation).

FIG. 9. Difference phase PSD, SMF to HCF comparison (before evacuation). In both cases, the HCF contribution (interferometer B) is scaled by $(\tau_A/\tau_B)^2 \approx 0.5$; the associated model curve (*) takes this scaling into account. The "sum" curve represents the total noise model: SMF, HCF, and measurement noise (not shown). The vibration contribution (< 20 kHz) was particularly weak for "SMF vs HCF #2," perhaps because of favorable laboratory conditions at the moment this specific measurement was taken.
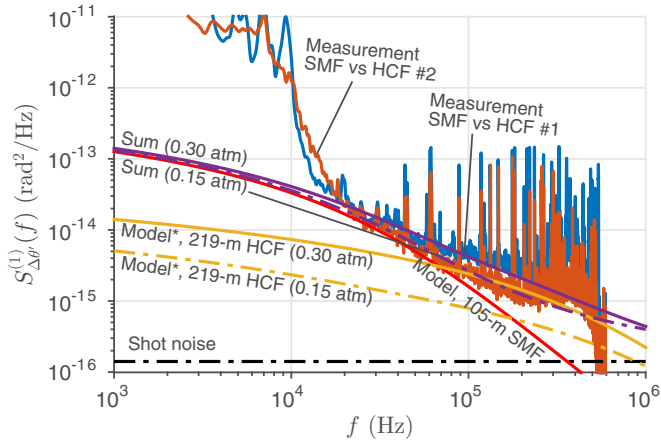
FIG. 10. Difference phase PSD, SMF to HCF comparison (after evacuation). In both cases, the HCF contribution (interferometer B) is scaled by $(\tau_A/\tau_B)^2 \approx 0.5$; the associated model curve (*) takes this scaling into account. The solid lines are for the first HCF, the dashed-dotted lines for the second HCF (longer evacuation). The "sum" curves represent the total noise model: SMF, HCF, and measurement noise (not shown).

FIG. 11. Difference phase PSD, HCF to HCF comparison (before and after evacuation). The "sum" curve represents the total noise model: HCF, HCF, and measurement noise (not shown).

broadly consistent with one another. Obviously, we cannot rule out the possibility that the internal pressure is actually 1 atm and that the noise model is inaccurate. However, tuning only the mode-field radius or thermo-optic coefficient (for example) does not improve the match as well as simply reducing the internal pressure, which we take as an argument to favor the latter explanation. Moreover, the HCF samples were given several weeks to attain thermal equilibrium with the laboratory environment, and laser power absorbed within the core cannot significantly increase the gas temperature under our experimental conditions [55]; the large temperature error (larger than 60 °C) which would be required to explain the observed discrepancy in Fig. 8 is therefore unrealistic.

We then set out to verify the central assumption of the adapted thermoconductive noise model, which is that the noise is driven by the thermo-optic contribution from the gas inside the core. Following a procedure presented in [68], we unsealed the first HCF and inserted the fiber end into a vacuum chamber so as to lower the internal gas pressure, heating the whole 219-m fiber to 70 °C to accelerate the evacuation process. After two weeks, we re-spliced the connector (thus sealing the fiber) and let the fiber cool down to room temperature. During the splicing operation, the HCF was left open to the atmosphere for approximately 15 min, allowing some ingress of atmospheric air. The phase noise of this partially evacuated fiber, interferometrically compared to a SMF fiber, is shown in Fig. 10 (SMF vs HCF #1). Although there is a lot of contamination by high-frequency tones in this specific case (these are also visible in the measurement noise PSD, which is not shown, suggesting that these are not due to the fiber samples themselves; these high-frequency tones appear in an intermittent fashion and are thought to couple through some of the preamplifiers), it is still clear that SMF thermal noise dominates the total phase noise between 20 and 100 kHz. Moreover, a reasonable match between measurement and model is attained by assuming that the HCF's
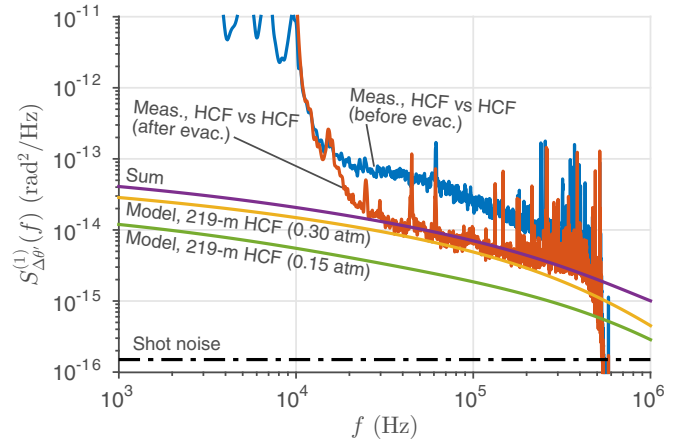
internal pressure is 0.30 atm (solid "sum" curve). We then repeated the procedure for the second HCF sample, leaving the open fiber end in the vacuum chamber for 6 weeks. This time, we significantly improved the splicing procedure and managed to seal the fiber within 4 min. This fiber's noise PSD, still compared to that of the reference SMF, is also shown in Fig. 10 (SMF vs HCF No. 2); its level is slightly below that of the first HCF and reasonably matches the thermal noise model if we assume $p = 0.15$ atm (dashed "sum" curve). Finally, we compared the HCFs to one another in order to remove the dominant SMF contribution (Fig. 11). Clearly, venting the HCFs lowered the phase noise PSD and slightly modified its spectral shape, as predicted by the model. Moreover, the total PSD is well represented by the two pressures guessed from the comparisons to SMF in Fig. 10. From numerical simulations (Fig. 12), these two internal pressures (0.30 and 0.15 atm) appear physically reasonable given the evacuation time and the time it took to seal the fibers once their ends were exposed to the atmosphere.

Figure 13 constitutes a summary of the most important experimental results of this paper, displaying phase PSDs that are normalized to the total optical length. Even though it has a larger mode area, the HCF is noisier per unit optical length than a typical SMF, at least above approximately 10 kHz and when the internal pressure is close to atmospheric. Reducing the internal pressure reduces the noise as predicted by our model, yielding a normalized phase noise level below that of SMF between 20 and 75 kHz [assuming a pressure that is the average between that of the two evacuated samples, $(0.30 + 0.15)/2 \approx 0.23$ atm]. To the best of our knowledge, the normalized phase noise in this spectral range is the lowest ever measured in a fiber. Our model predicts that this improvement with respect to SMF should extend to lower frequencies, but our measurements are contaminated by environmental fluctuations in this spectral range, preventing a definitive conclusion. Finally, if we were able to isolate only the contribution from the better-evacuated HCF, for which we infer an internal pressure of 0.15 atm, we would expect to see that the HCF is significantly quieter than a typical SMF below 100 kHz (lowermost curve at low frequencies).
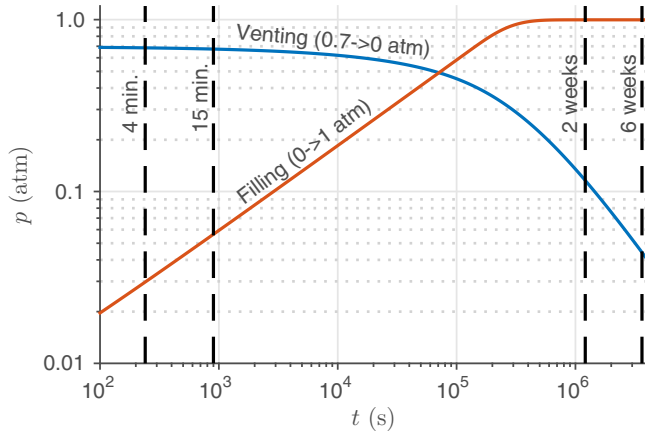
FIG. 12. Numerical solution to the diffusion equation in the hydrodynamic regime (Poiseuille flow) for a 219-m HCF open at a single end [48]. Only the properties of nitrogen (N_2) are considered. Venting is performed at $70\,°C$ in a fiber with an initial pressure that is spatially uniform at a level of 0.7 atm. Filling is performed at $20\,°C$ and assumes a perfectly evacuated fiber is suddenly exposed to atmospheric pressure at one open end. The displayed pressure is the spatial average over the fiber length (steady-state distribution after sealing) and the capillary diameter is assumed to be equal to the HCF's core diameter, $d \approx 35\ \mu m$. This model only provides a rough estimate of the relevant timescales since the initial filling pressure is not properly considered, since the diffusion equation becomes inaccurate as the slip-flow regime is approached below 0.2 atm (slows down processes), since the gas should be assumed to be compressible (speeds up processes), and since the core is not cylindrical like assumed here (slows down processes) [69].

IV. DISCUSSION

To our knowledge, measurement of fundamental thermal noise in a HCF has only been previously reported by Cranch *et al.* [32]. The authors built a balanced Mach-Zehnder interferometer with hollow-core photonic band-gap fibers (PBGF): a 10-m sample of HC1550 (NKT, $a = 4.5\ \mu m$) in one arm and a 10-m sample of HC19 (NKT, $a = 6.5\ \mu m$) in the other arm. In contrast to the approach used here, they held the
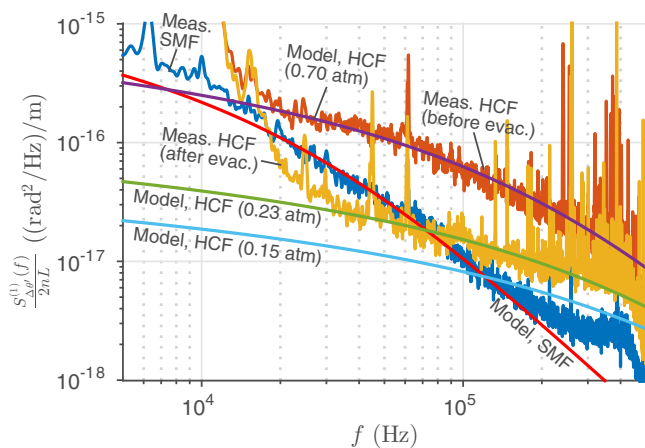

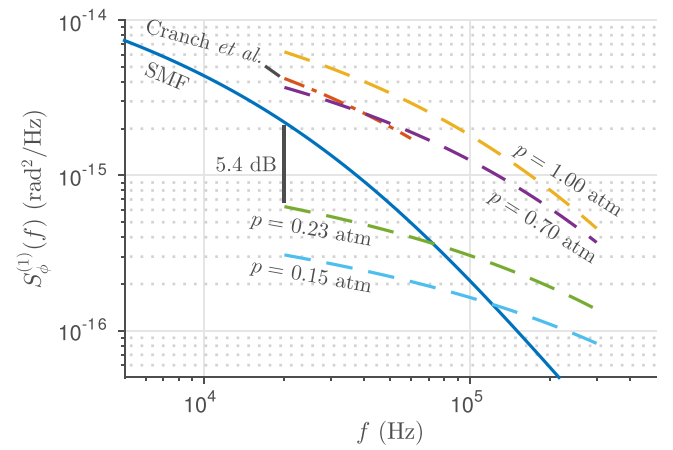FIG. 13. Optical-length-normalized phase PSD. Summary of the main experimental results.

FIG. 14. Phase PSD at $\lambda = 1550$ nm for $nL = 20$ m. The solid blue curve is the thermoconductive noise model for a standard SMF with $a = 5.25\ \mu m$. The HCF noise measured by Cranch *et al.* for $nL = 2 \times 10$ m is shown in dashed-dotted orange; it is a few dBs below their reference curve, calculated with $nL = 29$ m and $a = 2.61\ \mu m$, in the 20 to 60 kHz range (not shown), but a few dBs above the noise of a typical SMF of equal optical length (solid blue). The dashed yellow, purple, green, and teal curves represent the thermoconductive noise model for our large-mode-area HCF sample, normalized to the same 20-m optical length, at 1.00, 0.70, 0.23, and 0.15 atm, respectively.

interferometer at the quadrature point to measure the phase fluctuations. Although the measured noise spectrum in the 100 Hz to 100 kHz range changed over time, a phenomenon attributed to multipath interference due to higher-order mode propagation, the minimum noise level in the 20 to 60 kHz range was shown to be approximately 2 dB lower than the thermoconductive phase noise of a reference SMF with the same physical length L (and thus larger optical length nL), but only a few dBs above the detector noise. As stated in [32], the parameters of the reference SMF are described by Bartolo *et al.* [46]. While the minimum HCF noise measured by Cranch *et al.* is lower than the thermal noise of their reference SMF, the difference narrows to 0.4 dB when the phase PSD is normalized by the optical length $[2-10 \log_{10}(1.45) = 0.4$ dB], which we consider to be the fairest basis of comparison as explained in Sec. II. Moreover, their reference SMF has an anomalously small mode-field radius $a = 2.61\ \mu m$ (e^{-2}), much below the mode-field radius of their two HCF samples or that of a standard SMF used in the telecommunications field. The noise they measured, as far as we can tell, is thus 3 to 5 dB above that of a standard SMF ($a = 5.25\ \mu m$) of equal optical length and is comparable to the noise we measured in a large-mode-area HCF at an internal pressure of 0.7 atm (Fig. 14). Although the PSD they measured is lower than that predicted by the model we developed here (when accounting for the mode-field radii), it is likely also limited by the atmospheric air inside the HCF since there is no evidence that the HCFs were evacuated. The discrepancy between our model and their measurements could be explained by the observed multipath interference: higher-order modes should sample apparent temperature fluctuations that are similar to those seen
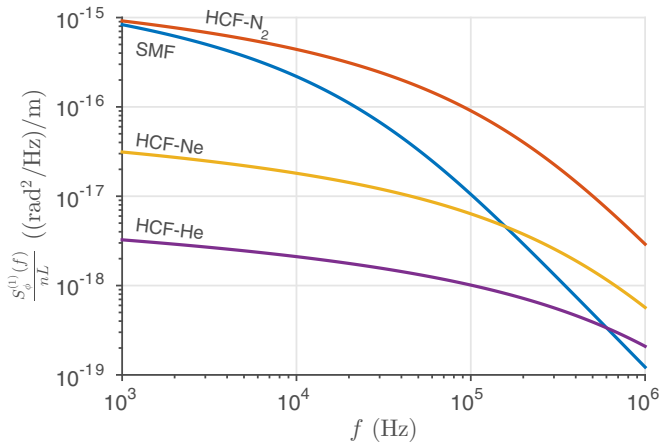
FIG. 15. Modeled optical-length-normalized phase PSD at $\lambda = 1539.8$ nm. Comparison between SMF and HCF filled with different species (nitrogen, N_2; neon, Ne; helium, He) at a pressure of 1 atm. A mode field radius $a = 5.25$ μm is considered for the SMF and $a = 12.5$ μm for the HCFs. The curve for helium can be considered to constitute a noise ceiling since this molecule would normally out diffuse of the hollow core over time, leaving a vacuum.

by the fundamental mode. Heuristically, it is therefore possible for the minimum noise to be smaller than that which would be found in the fundamental mode only (because of interference), preventing an adequate estimate of fundamental thermal noise. In any case, it is clear that the newer generation HCF used here does not display such multipath interference and, when held at an internal pressure of 0.23 atm, displays fundamental thermal noise that is up to 5.4 dB weaker than that of a typical SMF in the 20 to 60 kHz range. This is due in part to the mode with a large area in the HCF we used, but this remains true up to 40 kHz even if we force identical mode areas in SMF and HCF (3.3 dB instead of 5.4 dB weaker noise at 20 kHz).

Until now, it has been assumed that the hollow-core fiber is filled with nitrogen since it very well approximates the thermal and optical behavior of air while being much simpler to model. Yet, it is possible to fill a HCF with other gases than air, and the equations presented in Sec. II B show how this can yield a phase-noise reduction even if the core pressure is maintained at 1 atm. From Eq. (12), the thermo-optic coefficient is directly proportional to the polarizability α; in general, lighter molecules should thus produce smaller phase noise for a given pressure and temperature. Optimizing the thermal properties is somewhat more difficult since an assumption must be made about the frequency range of operation. Let us suppose once again that we are interested in frequencies below the cutoff so that $Q(f) \propto c_v/k_t$ [Eq. (14)]. From Eq. (13), we can then identify k_t/α^2 as a useful figure of merit for gases. This figure of merit appears to be maximized in helium [53,59], a molecule small enough to diffuse through the silica cladding and out of the hollow core over a reasonable time frame [70]; this constitutes a positive side effect since phase noise is also proportional to pressure. In theory, neon gas is also associated to a lower noise PSD than nitrogen (Fig. 15), while argon is only slightly better (not illustrated). Hence, filling a HCF

with gaseous He or Ne appears as a promising approach to minimize phase noise and improve the fundamental length stability. Nevertheless, such predictions have to be verified experimentally since the simplifying assumptions made here may break down and since other forms of noise may become dominant as thermoconductive noise is lowered below the 10^{-17} (rad^2/Hz)/m mark, the lowest measured value here (see Fig. 13).

V. CONCLUSION

In summary, we measured fundamental thermal noise in the latest generation of antiresonant hollow-core fibers using 219-m samples and high-throughput photodetectors to minimize shot noise and attain an adequate dynamic range. We found that the spectrum of this noise is distinct in both shape and level from that measured in standard solid-core silica fibers (SMF). Moreover, it is well explained by an adapted thermoconductive noise model, which only considers the thermal and thermo-optic properties of the gas trapped within the hollow core, in the 20 to 200 kHz frequency range and 0.1 to 1 atm pressure range. For equal mode-field areas and optical lengths, we showed that an antiresonant HCF at atmospheric pressure displays significantly larger thermoconductive phase noise than a SMF, at least at frequencies above 1 kHz. Yet, the model we developed also indicates that this noise can be lowered by filling the core with low-polarizability gas such as neon or helium or by simply evacuating the core, a prediction supported by the experiments we performed over partially vented HCF samples. At an internal pressure approaching 0.2 atm and around 30 kHz, our measurements reveal the lowest phase noise PSD per unit optical length ever measured in a fiber, 1.3×10^{-17} (rad^2/Hz)/m.

These results should help refine the estimation of the fundamental noise floor in instruments already based on HCF, for example, photothermal interferometers, but also in those instruments which can benefit from an SMF-to-HCF switch such as fiber-optic gyroscopes, optical fiber links, optoelectronic oscillators, and fiber interferometers used for laser frequency stabilization. In all related applications, a large-mode-area NANF at a subatmospheric internal pressure may surpass standard SMF in terms of fundamental optical length stability. Although a more elaborate noise model and better low-frequency measurements are required to quantify the extent of the potential improvement, an order of magnitude gain already appears within reach in the 10 to 100 kHz range. This high-stability potential comes in addition to other desirable properties of NANF such as high purity of polarization [71], low nonlinearity [72], weak backscattering [60], and low thermal sensitivity [44] (which can all benefit from core evacuation) in antiresonant HCFs displaying a transmission loss competitive with SMF at 1550 nm [33] and lower than SMF below 1100 nm [73]. Kilometer-scale antiresonant hollow-core fibers, properly shielded from environmental fluctuations and illuminated by high laser power, can therefore be considered for the most demanding interferometric applications.

The data for this work are accessible through the University of Southampton Institutional Research Repository [74].

ACKNOWLEDGMENTS

[1] V. Dangui, H. K. Kim, M. J. F. Digonnet, and G. S. Kino, Phase sensitivity to temperature of the fundamental mode in air-guiding photonic-bandgap fibers, Opt. Express **13**, 6669 (2005).

[2] R. Slavík, G. Marra, E. Numkam Fokoua, N. Baddela, N. V. Wheeler, M. Petrovich, F. Poletti, and D. J. Richardson, Ultralow thermal sensitivity of phase and propagation delay in hollow core optical fibres, Sci. Rep. **5**, 15447 (2015).

[3] W. H. Glenn, Noise in interferometric optical systems: An optical Nyquist theorem, IEEE J. Quantum Electron. **25**, 1218 (1989).

[4] K. H. Wanser, Fundamental phase noise limit in optical fibres due to temperature fluctuations, Electron. Lett. **28**, 53 (1992).

[5] S. Foster, Dynamical noise in single-mode distributed feedback fiber lasers, IEEE J. Quantum Electron. **40**, 1283 (2004).

[6] J. Lim, A. A. Savchenkov, E. Dale, W. Liang, D. Eliyahu, V. Ilchenko, A. B. Matsko, L. Maleki, and C. W. Wong, Chasing the thermodynamical noise limit in whispering-gallery-mode resonators for ultrastable laser frequency stabilization, Nat. Commun. **8**, 8 (2017).

[7] S. Foster, A. Tikhomirov, and M. Milnes, Fundamental thermal noise in distributed feedback fiber lasers, IEEE J. Quantum Electron. **43**, 378 (2007).

[8] G. Gagliardi, M. Salza, S. Avino, P. Ferraro, and P. De Natale, Probing the ultimate limit of fiber-optic strain sensing, Science **330**, 1081 (2010).

[9] S. Knudsen, A. B. Tveten, and A. Dandridge, Measurements of fundamental thermal induced phase fluctuations in the fiber of a Sagnac interferometer, IEEE Photonics Technol. Lett. **7**, 90 (1995).

[10] Y. Li, Y. Cao, D. He, Y. Wu, F. Chen, C. Peng, and Z. Li, Thermal phase noise in giant interferometric fiber optic gyroscopes, Opt. Express **27**, 14121 (2019).

[11] P. A. Williams, W. C. Swann, and N. R. Newbury, High-stability transfer of an optical frequency over long fiber-optic links, J. Opt. Soc. Am. B **25**, 1284 (2008).

[12] F. Stefani, O. Lopez, A. Bercy, W.-K. Lee, C. Chardonnet, G. Santarelli, P.-E. Pottie, and A. Amy-Klein, Tackling the limits of optical fiber links, J. Opt. Soc. Am. B **32**, 787 (2015).

[13] J. P. Cahill, W. Zhou, and C. R. Menyuk, Additive phase noise of fiber-optic links used in photonic microwave-generation systems, Appl. Opt. **56**, B18 (2017).

[14] F. Kéfélian, H. Jiang, P. Lemonde, and G. Santarelli, Ultralow-frequency-noise stabilization of a laser by locking to an optical fiber-delay line, Opt. Lett. **34**, 914 (2009).

[15] J. Dong, Y. Hu, J. Huang, M. Ye, Q. Qu, T. Li, and L. Liu, Subhertz linewidth laser by locking to a fiber delay line, Appl. Opt. **54**, 1152 (2015).

[16] S. Foster, Low-frequency thermal noise in optical fiber cavities, Phys. Rev. A **86**, 043801 (2012).

[17] W. B. Gardner, Microbending loss in optical fibers, Bell Syst. Tech. J. **54**, 457 (1975).

[18] W. Zhu, E. R. Numkam Fokoua, A. A. Taranta, Y. Chen, T. D. Bradley, M. N. Petrovich, F. Poletti, M. Zhao, D. J. Richardson, and R. Slavík, The thermal phase sensitivity of both coated and uncoated standard and hollow core fibers down to cryogenic temperatures, J. Lightwave Technol. **38**, 2477 (2020).

[19] B. Merkel, D. Repp, and A. Reiserer, Laser stabilization to a cryogenic fiber ring resonator, Opt. Lett. **46**, 444 (2021).

[20] S. Foster, G. A. Cranch, and A. Tikhomirov, Experimental evidence for the thermal origin of $1/f$ frequency noise in erbium-doped fiber lasers, Phys. Rev. A **79**, 053802 (2009).

[21] R. Kashyap, S. Hornung, M. H. Reeve, and S. A. Cassidy, Temperature desensitisation of delay in optical fibres for sensor applications, Electron. Lett. **19**, 1039 (1983).

[22] T. Iwashima, A. Inoue, M. Shigematsu, M. Nishimura, and Y. Hattori, Temperature compensation technique for fibre Bragg gratings using liquid crystalline polymer tubes, Electron. Lett. **33**, 417 (1997).

[23] M. Bousonville, M. K. Bock, M. Felber, T. Ladwig, T. Lamb, H. Schlarb, S. Schulz, C. Sydlo, S. Hunziker, P. Kownacki, and S. Jablonski, New phase stable optical fiber, in *Proceedings of the Paper presented at Beam Instrumentation Workshop 2012 (BIW2012), Newport News, VA, USA* (Jefferson Lab, 2012), paper MOPG033, pp. 101–103

[24] D. L. Weidman, G. H. Beall, K. C. Chyung, G. L. Francis, R. A. Modavis, and R. M. Morena, A novel negative expansion substrate material for athermalizing fiber Bragg gratings, in *Proceedings of European Conference on Optical Communication*, Vol. 1 (IEEE, Piscataway, NJ, 1996), pp. 61–64.

[25] M. Ding, E. R. Numkam Fokoua, T. D. Bradley, F. Poletti, D. J. Richardson, and R. Slavík, Hollow core fiber temperature sensitivity reduction via winding on a thermally-insensitive coil, in *CLEO: Science and Innovations* (Optical Society of America, Washington, DC, 2021), p. STu1Q–7.

[26] K. Shima, K. Himeno, T. Sakai, S. Okude, A. Wada, and R. Yamauchi, A novel temperature-insensitive long-period fiber grating using a boron-codoped-germanosilicate-core fiber, in *Proceedings of Optical Fiber Communication Conference* (IEEE, Piscataway, NJ, 1997), pp. 347–348.

[27] Z. Feng, V. Michaud-Belleau, J. K. Sahu, J. Nilsson, C. A. Codemard, X. Zhang, J. Genest, D. J. Richardson, and R. Slavík, Fiber interferometry with low temperature sensitivity, in *2020 IEEE Photonics Conference (IPC)* (IEEE, Piscataway, NJ, 2020), pp. 1–2.

[28] F. Poletti, Nested antiresonant nodeless hollow core fiber, Opt. Express **22**, 23807 (2014).

[29] G. Beck, L. Bigot, G. Bouwmans, A. Kudlinski, J.-P. Vilcot, and M. Douay, Benefits of photonic bandgap fibers for the thermal stabilization of optoelectronic oscillators, IEEE Photonics J. **4**, 789 (2012).

[30] S. Meiselman and G. A. Cranch, Optical phase response to temperature in a hollow-core photonic crystal fiber, Opt. Express **25**, 27581 (2017).

[31] R. Slavík, E. R. Numkam Fokoua, M. Bukshtab, Y. Chen, T. D. Bradley, S. R. Sandoghchi, M. N. Petrovich, F. Poletti, and D. J. Richardson, Demonstration of opposing thermal sensitivities in hollow-core fibers with open and sealed ends, Opt. Lett. **44**, 4367 (2019).

[32] G. A. Cranch and G. A. Miller, Coherent light transmission properties of commercial photonic crystal hollow core optical fiber, Appl. Opt. **54**, F8 (2015).

[33] G. T. Jasion, T. D. Bradley, K. Harrington, H. Sakr, Y. Chen, E. Numkam Fokoua, I. A. Davidson, A. Taranta, J. R. Hayes, D. J. Richardson, and F. Poletti, Hollow core NANF with 0.28 dB/km attenuation in the C and L bands, in *Optical Fiber Communication Conference* (Optical Society of America, Washington, DC, 2020), p. Th4B–4.

[34] W. Ding, Y.-Y. Wang, S.-F. Gao, M.-L. Wang, and P. Wang, Recent progress in low-loss hollow-core anti-resonant fibers and their applications, IEEE J. Sel. Top. Quantum Electron. **26**, 1 (2019).

[35] H. B. Callen and R. F. Greene, On a theorem of irreversible thermodynamics, Phys. Rev. **86**, 702 (1952).

[36] S. Foster, Fundamental limits on $1/f$ frequency noise in rare-earth-metal-doped fiber lasers due to spontaneous emission, Phys. Rev. A **78**, 013820 (2008).

[37] G. Agrawal, *Nonlinear Fiber Optics* (Elsevier, Amsterdam, 2012).

[38] L. Duan, General treatment of the thermal noises in optical fibers, Phys. Rev. A **86**, 023817 (2012).

[39] M. L. Gorodetsky and I. S. Grudinin, Fundamental thermal fluctuations in microspheres, J. Opt. Soc. Am. B **21**, 697 (2004).

[40] V. B. Braginsky, M. L. Gorodetsky, and S. P. Vyatchanin, Thermo-refractive noise in gravitational wave antennae, Phys. Lett. A **271**, 303 (2000).

[41] T. Kessler, T. Legero, and U. Sterr, Thermal noise in optical cavities revisited, J. Opt. Soc. Am. B **29**, 178 (2012).

[42] L. Duan, Thermal noise-limited fiber-optic sensing at infrasonic frequencies, IEEE J. Quantum Electron. **51**, 1 (2014).

[43] J. Dong, J. Huang, T. Li, and L. Liu, Observation of fundamental thermal noise in optical fibers down to infrasonic frequencies, Appl. Phys. Lett. **108**, 021108 (2016).

[44] B. Shi, H. Sakr, J. Hayes, X. Wei, E. Numkam Fokoua, M. Ding, Z. Feng, G. Marra, F. Poletti, D. J. Richardson, and R. Slavík, Thinly coated hollow core fiber for improved thermal phase-stability performance, Opt. Lett. **46**, 5177 (2021).

[45] J. Song, K. Sun, S. Li, and W. Cai, Phase sensitivity to temperature of the guiding mode in polarization-maintaining photonic crystal fiber, Appl. Opt. **54**, 7330 (2015).

[46] R. E. Bartolo, A. B. Tveten, and A. Dandridge, Thermal phase noise measurements in optical fiber interferometers, IEEE J. Quantum Electron. **48**, 720 (2012).

[47] Y. Lin, W. Jin, F. Yang, J. Ma, C. Wang, H. L. Ho, and Y. Liu, Pulsed photothermal interferometry for spectroscopic gas detection with hollow-core optical fibre, Sci. Rep. **6**, 39410 (2016).

[48] J. Henningsen and J. Hald, Dynamics of gas flow in hollow core photonic bandgap fibers, Appl. Opt. **47**, 2790 (2008).

[49] T. L. Bergman, A. S. Lavine, F. P. Incropera, and D. P. DeWitt, *Introduction to Heat Transfer* (Wiley, Hoboken, NJ, 2011).

[50] B. Edlén, The refractive index of air, Metrologia **2**, 71 (1966).

[51] M. Zeisberger and M. A. Schmidt, Analytic model for the complex effective index of the leaky modes of tube-type anti-resonant hollow core fibers, Sci. Rep. **7**, 11761 (2017).

[52] S. J. Blundell and K. M. Blundell, *Concepts in Thermal Physics* (Oxford University Press, Oxford, 2010).

[53] J. W. Haarman, Thermal conductivity measurements of He, Ne, Ar, Kr, N_2 and CO_2 with a transient hot wire method, in *AIP Conference Proceedings*, Vol. 11 (American Institute of Physics, New York, 1973), pp. 193–202.

[54] H. H. Uhlig and F. G. Keyes, The dependence of the dielectric constants of gases on temperature and density, J. Chem. Phys. **1**, 155 (1933).

[55] C. C. Davis and S. J. Petuchowski, Phase fluctuation optical heterodyne spectroscopy of gases, Appl. Opt. **20**, 2539 (1981).

[56] J. R. Barker and T. Rothem, Theory of the time-dependent-thermal-lensing (TDTL) technique as used in energy-transfer experiments, Chem. Phys. **68**, 331 (1982).

[57] W. Jin, Y. Cao, F. Yang, and H. L. Ho, Ultra-sensitive all-fibre photothermal spectroscopy with large dynamic range, Nat. Commun. **6**, 6767 (2015).

[58] K. Krzempek, A review of photothermal detection techniques for gas sensing applications, Appl. Sci. **9**, 2826 (2019).

[59] M. A. Buldakov, I. I. Matrosov, and V. N. Cherepanov, Temperature dependence of polarizability of diatomic homonuclear molecules, Opt. Spectrosc. **89**, 37 (2000).

[60] V. Michaud-Belleau, E. Numkam Fokoua, T. D. Bradley, J. R. Hayes, Y. Chen, F. Poletti, D. J. Richardson, J. Genest, and R. Slavík, Backscattering in antiresonant hollow-core fibers: over 40 dB lower than in standard optical fibers, Optica **8**, 216 (2021).

[61] V. Michaud-Belleau, M. Charlet, A. Tourigny-Plante, J.-D. Deschênes, and J. Genest, External serrodyne modulation for the suppression of low-frequency noise in quadrature interferometry, Opt. Lett. **45**, 670 (2020).

[62] V. Michaud-Belleau, J. Genest, and J.-D. Deschênes, Optimal Detection Scheme for Shot-Noise-Limited Phase Estimation in Passive Classical-Light Interferometry, Phys. Rev. Appl. **10**, 024025 (2018).

[63] G. Skolianos, A. Arora, M. Bernier, and M. J. F. Digonnet, Photonics sensing at the thermodynamic limit, Opt. Lett. **42**, 2018 (2017).

[64] V. Michaud-Belleau, H. Bergeron, P. S. Light, N. B. Hébert, J.-D. Deschênes, A. N. Luiten, and J. Genest, Passive coherent discriminator using phase diversity for the simultaneous measurement of frequency noise and intensity noise of a continuous-wave laser, Metrologia **53**, 1154 (2016).

[65] M. Pang, H. F. Xuan, J. Ju, and W. Jin, Influence of strain and pressure to the effective refractive index of the fundamental mode of hollow-core photonic band gap fibers, Opt. Express **18**, 14041 (2010).

[66] S. Rikimi, Y. Chen, T. W. Kelly, I. A. Davidson, G. T. Jasion, M. Partridge, K. Harrington, T. D. Bradley, A. A. Taranta, F. Poletti, M. N. Petrovich, D. J. Richardson, and N. V. Wheeler, Internal gas composition and pressure in as-drawn hollow core optical fibers, J. Lightwave Technol. **40**, 4776 (2022).

[67] I. Dicaire, J.-C. Beugnot, and L. Thévenaz, Analytical modeling of the gas-filling dynamics in photonic crystal fibers, Appl. Opt. **49**, 4604 (2010).

[68] E. A. Curtis, T. Bradley, G. P. Barwood, C. S. Edwards, N. V. Wheeler, R. Phelan, D. J. Richardson, M. N. Petrovich, and P. Gill, Laser frequency stabilization and spectroscopy at 2051 nm using a compact CO_2-filled Kagome hollow core fiber gas-cell system, Opt. Express **26**, 28621 (2018).

[69] P. Bojęś, P. Jaworski, K. Krzempek, Z. Malecha, F. Yu, D. Wu, P. Kozioł, G. Dudzik, M. Liao, and K. Abramski, Experimental

and numerical analysis of gas flow in nodeless antiresonant hollow-core fibers for optimization of laser gas spectroscopy sensors, Opt. Laser Technol. **152**, 108157 (2022).

[70] F. Benabid, P. S. Light, and F. Couny, Low insertion-loss (1.8 dB) and vacuum-pressure all-fiber gas cell based on hollow-core PCF, in *The European Conference on Lasers and Electro-Optics* (Optical Society of America, Washington, DC, 2007), p. CH_3.

[71] A. Taranta, E. Numkam Fokoua, S. A. Mousavi, J. R. Hayes, T. D. Bradley, G. T. Jasion, and F. Poletti, Exceptional polarization purity in antiresonant hollow-core optical fibres, Nat. Photonics **14**, 504 (2020).

[72] S. A. Mousavi, H. C. H. Mulvad, N. V. Wheeler, P. Horak, J. Hayes, Y. Chen, T. D. Bradley, S. Alam, S. R. Sandoghchi, E. Numkam Fokoua, D. J. Richardson, and F. Poletti, Nonlinear dynamic of picosecond pulse propagation in atmospheric air-filled hollow core fibers, Opt. Express **26**, 8866 (2018).

[73] H. Sakr, Y. Chen, G. T. Jasion, T. D. Bradley, J. R. Hayes, H. C. H. Mulvad, I. A. Davidson, E. Numkam Fokoua, and F. Poletti, Hollow core optical fibres with comparable attenuation to silica fibres between 600 and 1100 nm, Nat. Commun. **11**, 6030 (2020).

[74] doi:10.5258/SOTON/D2301.